Proceedings of the 2025 SICE Festival with Annual Conference
September 9-12, 2025, Chiang Mai, Thailand

Cooperative Payload Transportation Control for Multiple Fully-Actuated UAVs Based on Conic Control Barrier Functions

Shuta Ichitani† and Tatsuya Ibuki[1]

[1]Department of Electronics and Bioinformatics, Meiji University, Kanagawa, Japan
(Tel: +81-44-934-7344; E-mail: ibuki@meiji.ac.jp)

Abstract: This paper presents a cooperative load transportation system using multiple multirotor UAVs, with a focus on collision avoidance between the UAVs. Each aerial vehicle modeled as a fully-actuated UAV is connected to a payload via cables. In such a system, there is a risk of the UAVs' colliding with each other. To address this issue, the present method introduces collision avoidance constraints based on a conic control barrier function, applied individually in the direction of each cable. The control inputs for each UAV are then obtained by solving a constrained optimization problem. The effectiveness of the proposed method is demonstrated through simulations.

Keywords: Cooperative transportation, UAV, Suspended payload, Optimization, Control barrier function

1. INTRODUCTION

Recently, the demand for multirotor UAVs, such as quadrotors and hexarotors, has rapidly increased due to their cost-effectiveness and operational simplicity. Their applications are diverse, ranging from infrastructure inspections [1], construction sites [2], and entertainment [3]. UAVs are particularly promising for load transportation, especially in depopulated areas and remote islands with limited logistical access. Their high agility and vertical movement capabilities make them ideal for rapidly delivering critical supplies like medicine.

Research into UAVs transportation methods is ongoing, and there are two main types. The first type directly attaches the payload to the UAV [4, 5], while the second is a suspended-type, where the payload is hung from the UAV via a cable. The former approach constrains payload sizes and shapes due to the UAV's structural limitations, which adversely affects maneuverability by increasing the overall inertia of the airframe. In contrast, the suspended-type accommodates various payload configurations and enables the use of multiple UAVs for cooperative transportation. This also enhances fault tolerance, as remaining UAVs can compensate for potential failures. Consequently, the suspended-type approach is considered in many cases more suitable for load transportation, and thus this study focuses on a multiple UAVs suspended-type transportation system.

The suspended-type offers scalability concerning the number of UAVs, prompting extensive research on systems employing various UAVs configurations. Additionally, diverse payload shapes, such as a spherical or a rectangular shape, have been explored [6-11]. However, the risks of UAV collisions and cable entanglement are inherent, necessitating the implementation of collision avoidance constraints. Several control strategies have been proposed to address these issues. For instance, [9] proposes a strategy in which the formation of the UAVs and the payload is predetermined by explicitly specifying the desired angle of each cable. In addition, in [10], the control system imposes a constraint to ensure each cable remains within the outer 1/4 quadrant of the payload. These conservative configurations lead to unnecessary thrust generation that is not directly required for payload transportation, resulting in excessive energy consumption. This issue is a significant concern for UAVs, which have a limited battery. To address this issue, our approach defines a conical region based on the upward vector of the payload and keeping the cable within this region. This allows cables to point inward toward the payload while avoiding UAVs' collision. Allowing inward cable movement is expected to enable more efficient force distribution, potentially reducing unnecessary thrust and lowering battery consumption.

In this paper, we focus on suspended-type transportation using three UAVs and propose a system that controls the payload position and attitude while ensuring UAVs safety through collision avoidance. Collision avoidance for UAVs includes both avoiding collision between UAVs and avoiding collision between a UAV and a cable. The reason for using three UAVs is the minimum number to control the payload's attitude. The payload is assumed to be rectangular, reflecting its widespread use in industrial and logistical applications. Although the most common type of UAVs are the quadrotors, this study focuses on fully-actuated hexarotors, which can generate thrust in both vertical and horizontal directions [12], to simplify the problem in the proposed method[1]. Additionally, for the towing equipment used to suspend the payload, we adopt a cable, which is modeled as tension, being easy to construct in the real world.

A key feature of this research is designing a constraint for each cable by a conic control barrier function (CBF) [14]. This is a method of dynamically controlling the control input direction to remain within a part of the spherical surface. By adopting a conical shape, more flexible cables attitude control becomes possible.

† Shuta Ichitani is the presenter of this paper.

[1]For the standard quadrotor model, we can simply apply the 3D motion tracking controller of a quadrotor [13] as a local controller, similarly to the previous work [8].

Table 1: Definition of symbols

Symbol	Definition
Σ_w, Σ_L	Inertial frame, Body-fixed frame
$m_L \in \mathbb{R}$	Mass of payload
$m_i \in \mathbb{R}$	Mass of i-th UAV
$\boldsymbol{J}_L \in \mathbb{R}^{3\times3}$	Inertia matrix of payload
$\boldsymbol{x}_L, \boldsymbol{v}_L \in \mathbb{R}^3$	Position, Velocity of payload in Σ_w
$\boldsymbol{x}_i, \boldsymbol{v}_i \in \mathbb{R}^3$	Position, Velocity of i-th UAV in Σ_w
$\boldsymbol{R}_L \in SO(3)$	Rotation matrix of payload from Σ_w to Σ_L
$\boldsymbol{\Omega}_L \in \mathbb{R}^3$	Angular velocity of payload in Σ_L
$\boldsymbol{\omega}_i \in \mathbb{R}^3$	Angular velocity of i-th cable in Σ_w
$\boldsymbol{f}_i \in \mathbb{R}^3$	Thrust of i-th UAV in Σ_L
$\boldsymbol{\rho}_i \in \mathbb{R}^3$	Point of payload in Σ_L where i-th cable is attached
$l_i \in \mathbb{R}$	Length of i-th cable
$\boldsymbol{q}_i \in S^2$	Unit direction vector of i-th cable in Σ_w
$g \in \mathbb{R}$	Magnitude of gravitational acceleration
$\boldsymbol{u}_i \in \mathbb{R}^3$	Thrust input force for i-th UAV
$\boldsymbol{\Delta}_{x_L}, \boldsymbol{\Delta}_{x_i} \in \mathbb{R}^3$	Disturbance of position of payload and i-th UAV in Σ_w
$\boldsymbol{\Delta}_{\boldsymbol{R}_L} \in \mathbb{R}^3$	Disturbance of attitude of payload in Σ_w
$\boldsymbol{e_3} = [0\ 0\ 1]^\top \in \mathbb{R}^3$	Unit vector

2. PROBLEM SETTING

This section defines the problem setting of multiple UAVs transportation of a rigid payload suspended by cables, and outlines the control objective.

2.1. Model of three UAVs transportation

As shown in Fig. 1, this paper considers three UAVs connected to a rectangular payload via massless cables that do not stretch, twist, or deflect. The payload's origin is at the center of gravity in the frame Σ_L. Using the symbols shown in Table 1, the dynamics of this aerial transportation system are formulated using Lagrangian mechanics, as detailed in [15], and take the form

$$\begin{aligned}
&\boldsymbol{M}_q\left(\ddot{\boldsymbol{x}}_L + g\boldsymbol{e}_3\right) - \sum_{i=1}^{3} m_i \boldsymbol{q}_i \boldsymbol{q}_i^\top \boldsymbol{R}_L \hat{\boldsymbol{\rho}}_i \dot{\boldsymbol{\Omega}}_L \\
&= \boldsymbol{\Delta}_{x_L} + \sum_{i=1}^{3} \Big(\boldsymbol{u}_i^{\parallel} + \boldsymbol{\Delta}_{x_i}^{\parallel} + m_i l_i \|\boldsymbol{\omega}_i\|^2 \boldsymbol{q}_i \\
&\qquad - m_i \boldsymbol{q}_i \boldsymbol{q}_i^\top \boldsymbol{R}_L \hat{\boldsymbol{\Omega}}_L^2 \boldsymbol{\rho}_i \Big), \qquad (1) \\
&\left(\boldsymbol{J}_L - \sum_{i=1}^{3} m_i \hat{\boldsymbol{\rho}}_i \boldsymbol{R}_L^\top \boldsymbol{q}_i \boldsymbol{q}_i^\top \boldsymbol{R}_L \hat{\boldsymbol{\rho}}_i \right) \dot{\boldsymbol{\Omega}}_L \\
&+ \sum_{i=1}^{3} m_i \hat{\boldsymbol{\rho}}_i \boldsymbol{R}_L^\top \boldsymbol{q}_i \boldsymbol{q}_i^\top \left(\ddot{\boldsymbol{x}}_L + g\boldsymbol{e}_3 \right) + \hat{\boldsymbol{\Omega}}_L \boldsymbol{J}_L \boldsymbol{\Omega}_L \\
&= \boldsymbol{\Delta}_{R_L} + \sum_{i=1}^{3} \hat{\boldsymbol{\rho}}_i \boldsymbol{R}_L^\top \Big(\boldsymbol{u}_i^{\parallel} + \boldsymbol{\Delta}_{x_i}^{\parallel} \\
&\qquad + m_i l_i \left\|\boldsymbol{\omega}_i\right\|^2 \boldsymbol{q}_i - m_i \boldsymbol{q}_i \boldsymbol{q}_i^\top \boldsymbol{R}_L \hat{\boldsymbol{\Omega}}_L^2 \boldsymbol{\rho}_i \Big), \qquad (2)
\end{aligned}$$

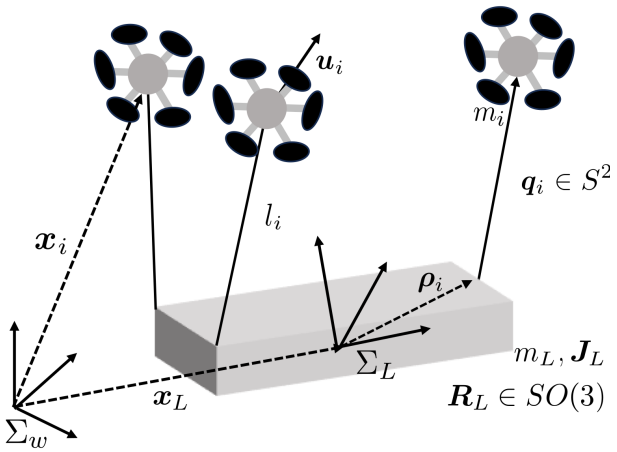

Fig. 1: Transportation system with three UAVs.

$$\begin{aligned}
\dot{\boldsymbol{\omega}}_i &= -\frac{1}{l_i}\hat{\boldsymbol{q}}_i \left(\ddot{\boldsymbol{x}}_L + g\boldsymbol{e}_3 - \boldsymbol{R}_L \hat{\boldsymbol{\rho}}_i \dot{\boldsymbol{\Omega}}_L + \boldsymbol{R}_L \hat{\boldsymbol{\Omega}}_L^2 \boldsymbol{\rho}_i \right) \\
&\quad + \frac{1}{m_i l_i} \hat{\boldsymbol{q}}_i \left(\boldsymbol{u}_i^{\perp} + \boldsymbol{\Delta}_{x_i}^{\perp} \right), \qquad (3) \\
\dot{\boldsymbol{R}}_L &= \boldsymbol{R}_L \hat{\boldsymbol{\Omega}}_L, \qquad (4) \\
\dot{\boldsymbol{q}}_i &= \hat{\boldsymbol{\omega}}_i \boldsymbol{q}_i. \qquad (5)
\end{aligned}$$

Here, $\boldsymbol{M}_q = m_L \boldsymbol{I}_3 + \Sigma_{i=1}^{n} m_i \boldsymbol{q}_i \boldsymbol{q}_i^\top \in \mathbb{R}^{3\times3}$, and $\boldsymbol{I}_3$ denotes the 3×3 identity matrix. Additionally, the wedge '$\wedge$': $\mathbb{R}^3 \to so(3)$, is defined so that $\hat{\boldsymbol{y}}\boldsymbol{z} = \boldsymbol{y} \times \boldsymbol{z}$ for all $\boldsymbol{y}, \boldsymbol{z} \in \mathbb{R}^3$, and the vee '$\vee$': $so(3) \to \mathbb{R}^3$, is defined the inverse of the wedge.

The control input of the present transportation system is thrust $\boldsymbol{u}_i$ of each UAV, which is divided into parallel and perpendicular components. The symbols '$\parallel$' and '$\perp$' denote the components of the vector that are parallel and perpendicular to $\boldsymbol{q}_i$, respectively. They are respectively defined as

$$\begin{aligned}
\boldsymbol{u}_i^{\parallel} &= \boldsymbol{q}_i \boldsymbol{q}_i^\top \boldsymbol{u}_i, \qquad (6) \\
\boldsymbol{u}_i^{\perp} &= -\hat{\boldsymbol{q}}_i^2 \boldsymbol{u}_i = \left(\boldsymbol{I}_3 - \boldsymbol{q}_i^\top \boldsymbol{q}_i \right). \qquad (7)
\end{aligned}$$

Furthermore, the relationship between these components is as follows:

$$\boldsymbol{u}_i = \boldsymbol{u}_i^{\parallel} + \boldsymbol{u}_i^{\perp}.$$

Similarly, the disturbance of position of i-th UAV is decomposed as

$$\begin{aligned}
\boldsymbol{\Delta}_{x_i}^{\parallel} &= \boldsymbol{q}_i \boldsymbol{q}_i^\top \boldsymbol{\Delta}_{x_i}, \qquad (8) \\
\boldsymbol{\Delta}_{x_i}^{\perp} &= -\hat{\boldsymbol{q}}_i^2 \boldsymbol{\Delta}_{x_i} = \left(\boldsymbol{I}_3 - \boldsymbol{q}_i^\top \boldsymbol{q}_i \right) \boldsymbol{\Delta}_{x_i}. \qquad (9)
\end{aligned}$$

2.2. Control objective

The control objective is to achieve position and attitude tracking control of the payload for their desired trajectories while ensuring safety by avoiding UAVs' collision and cable entanglements between a UAV and a cable. Collision avoidance is prioritized, followed by position and attitude tracking.

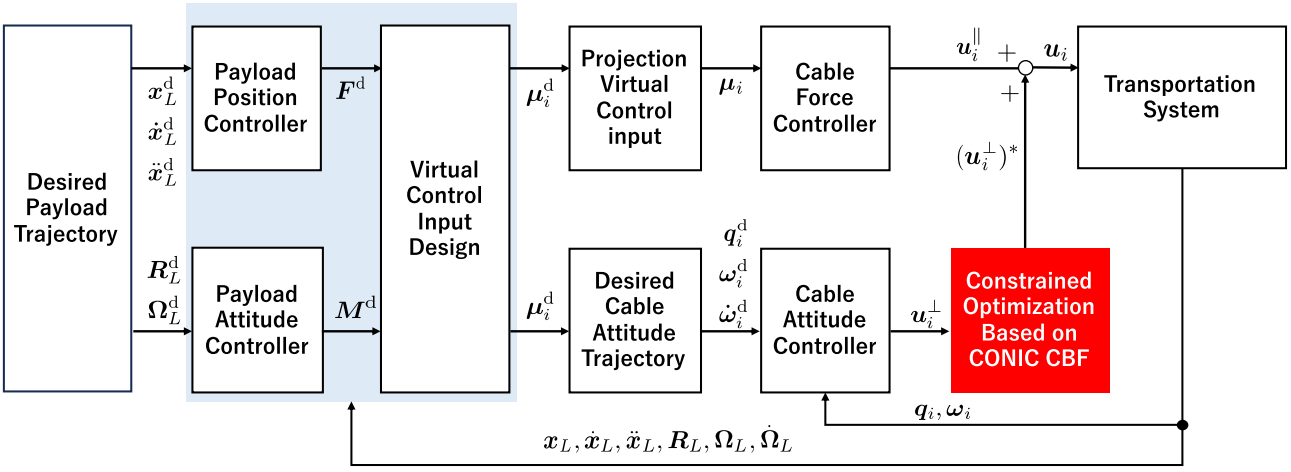

Fig. 2: Block diagram of entire control system

3. CONTROL SYSTEM DESIGN

In this section, we design the control input to transport a payload. Fig. 2 illustrates the block diagram of the entire control system. As mentioned previously, the control input consists of $\boldsymbol{u}_i^{\parallel}$ parallel to $\boldsymbol{q}_i$, and $\boldsymbol{u}_i^{\perp}$ perpendicular to $\boldsymbol{q}_i$. This is because only the force along the direction of the cable can influence the motion of the payload. Then, $\boldsymbol{u}_i^{\parallel}$ is designed such that the payload follows the desired position and attitude. $\boldsymbol{u}_i^{\perp}$ is designed so that the actual cable direction $\boldsymbol{q}_i$ follows the desired direction $\boldsymbol{q}_i^{\mathrm{d}} \in S^2$. The control system designed in this section is based on [8].

3.1. Design of parallel component

Since each UAV can exert force on the payload only along the direction of the cable, it is necessary to introduce the ideal tension force that each UAV should generate to control the payload under this constraint. To model this, we first define $\boldsymbol{a}_i \in \mathbb{R}^3$ as the acceleration of the point on the payload where the i-th link is connected. It is given as follows [8]:

$$\boldsymbol{a}_i = \ddot{\boldsymbol{x}}_L + g\boldsymbol{e}_3 + \boldsymbol{R}_L \hat{\boldsymbol{\Omega}}_L^2 \boldsymbol{\rho}_i - \boldsymbol{R}_L \hat{\boldsymbol{\rho}}_i \dot{\boldsymbol{\Omega}}_L. \tag{10}$$

Then, we introduce $\boldsymbol{\mu}_i \in \mathbb{R}^3$ as a virtual control input. It represents the force applied at the cable's attachment point on the payload, taking $\boldsymbol{q}_i$ into account. With this force specified, the parallel component of the control input is designed considering the force that has been generated as follows:

$$\boldsymbol{u}_i^{\parallel} = \boldsymbol{\mu}_i - m_i l_i \|\boldsymbol{\omega}_i\|^2 \boldsymbol{q}_i + m_i \boldsymbol{q}_i \boldsymbol{q}_i^{\top} \boldsymbol{a}_i. \tag{11}$$

Second, we define the desired control force $\boldsymbol{F}^{\mathrm{d}} \in \mathbb{R}^3$ and moment $\boldsymbol{M}^{\mathrm{d}} \in \mathbb{R}^3$ acting on the payload. This force is designed track the desired position and attitude trajectories of the payload. The control law is formulated using a PD-type approach as follows:

$$\begin{aligned}\boldsymbol{F}^{\mathrm{d}} = {} & m_L \left(-k_{x_L}\boldsymbol{e}_{x_L} - k_{\dot{x}_L}\dot{\boldsymbol{e}}_{\dot{x}_L} + \ddot{\boldsymbol{x}}_L^{\mathrm{d}} + g\boldsymbol{e}_3\right) \\ & - \bar{\boldsymbol{\Delta}}_{x_L} - \sum_{i=1}^{3} \bar{\boldsymbol{\Delta}}_{x_i}^{\parallel},\end{aligned} \tag{12}$$

$$\begin{aligned}\boldsymbol{M}^{\mathrm{d}} = {} & -\bar{\boldsymbol{\Delta}}_{\boldsymbol{R}_L} - k_{R_L}\boldsymbol{e}_{R_L} - k_{\Omega_L}\boldsymbol{e}_{\Omega_L} \\ & + \left(\boldsymbol{R}_L^{\top}\boldsymbol{R}_L^{\mathrm{d}}\boldsymbol{\Omega}_L^{\mathrm{d}}\right)^{\wedge} \boldsymbol{J}_L \boldsymbol{R}_L^{\top}\boldsymbol{R}_L^{\mathrm{d}}\boldsymbol{\Omega}_L^{\mathrm{d}} \\ & + \boldsymbol{J}_L \boldsymbol{R}_L^{\top}\boldsymbol{R}_L^{\mathrm{d}}\dot{\boldsymbol{\Omega}}_L^{\mathrm{d}} - \sum_{i=1}^{3} \hat{\boldsymbol{\rho}}_i \boldsymbol{R}_L \bar{\boldsymbol{\Delta}}_{x_i}^{\parallel},\end{aligned} \tag{13}$$

where $k_{x_L}, k_{\dot{x}_L}, k_{R_L}, k_{\Omega_L} > 0$ are positive gains. $\ddot{\boldsymbol{x}}_L^{\mathrm{d}} \in \mathbb{R}^3$ is the desired acceleration of the payload, and $\boldsymbol{R}_L^{\mathrm{d}}, \boldsymbol{\Omega}_L^{\mathrm{d}}, \dot{\boldsymbol{\Omega}}_L^{\mathrm{d}} \in \mathbb{R}^3$ are the desired attitude, angular velocity and acceleration, respectively of the payload. $\bar{\boldsymbol{\Delta}}_{x_L}, \bar{\boldsymbol{\Delta}}_{x_i}, \bar{\boldsymbol{\Delta}}_{R_L} \in \mathbb{R}^3$ are estimates of disturbances, and these will be provided in Section 3.3. Additionally, the position, attitude, and angular velocity tracking error vectors for the payload are

$$\begin{aligned}\boldsymbol{e}_{x_L} &= \boldsymbol{x}_L - \boldsymbol{x}_L^{\mathrm{d}}, \\ \boldsymbol{e}_{R_L} &= \frac{1}{2}\left((\boldsymbol{R}_L^{\mathrm{d}})^{\top}\boldsymbol{R}_L - \boldsymbol{R}_L^{\top}(\boldsymbol{R}_L^{\mathrm{d}})^{\top}\right)^{\vee}, \\ \boldsymbol{e}_{\Omega_L} &= \boldsymbol{\Omega}_L - \boldsymbol{R}_L^{\top}\boldsymbol{R}_L^{\mathrm{d}}\boldsymbol{\Omega}_L^{\mathrm{d}}.\end{aligned}$$

To generate the desired force and moment, we design a control scheme. However, each $\boldsymbol{\mu}_i$ is constrained to be parallel to $\boldsymbol{q}_i$. Therefore, we choose the desired a virtual control input $\boldsymbol{\mu}_i^{\mathrm{d}} \in \mathbb{R}^3$ to satisfy

$$\sum_{i=1}^{3} \boldsymbol{\mu}_i^{\mathrm{d}} = \boldsymbol{F}^{\mathrm{d}}, \quad \sum_{i=1}^{3} \hat{\boldsymbol{\rho}}_i \boldsymbol{R}_L^{\top} \boldsymbol{\mu}_i^{\mathrm{d}} = \boldsymbol{M}^{\mathrm{d}}. \tag{14}$$

These equations ensure that the sum of the virtual control inputs results in the desired force and moment.

Let us define a matrix $\boldsymbol{P} \in \mathbb{R}^{6\times 9}$ as follows:

$$\boldsymbol{P} = \begin{bmatrix} \boldsymbol{I}_3 & \boldsymbol{I}_3 & \boldsymbol{I}_3 \\ \hat{\boldsymbol{\rho}}_1 & \hat{\boldsymbol{\rho}}_2 & \hat{\boldsymbol{\rho}}_3 \end{bmatrix}. \tag{15}$$

Using the matrix $\boldsymbol{P}$, we can rewrite Eq. (14)

$$\boldsymbol{P} \begin{bmatrix} \boldsymbol{R}_L^{\top}\boldsymbol{\mu}_1^{\mathrm{d}} \\ \boldsymbol{R}_L^{\top}\boldsymbol{\mu}_2^{\mathrm{d}} \\ \boldsymbol{R}_L^{\top}\boldsymbol{\mu}_3^{\mathrm{d}} \end{bmatrix} = \begin{bmatrix} \boldsymbol{R}_L^{\top}\boldsymbol{F}^{\mathrm{d}} \\ \boldsymbol{M}^{\mathrm{d}} \end{bmatrix}. \tag{16}$$

We solve Eq. (16) for the desired virtual control input $\boldsymbol{\mu}_i^{\mathrm{d}}$ using the minimum-norm solution. The solution is given

by

$$\begin{bmatrix} \boldsymbol{\mu}_1^{\mathrm{d}} \\ \boldsymbol{\mu}_2^{\mathrm{d}} \\ \boldsymbol{\mu}_3^{\mathrm{d}} \end{bmatrix} = \mathrm{diag}[\boldsymbol{R}_L, \boldsymbol{R}_L, \boldsymbol{R}_L]\boldsymbol{P}^\top(\boldsymbol{P}\boldsymbol{P}^\top)^{-1} \begin{bmatrix} \boldsymbol{R}_L^\top \boldsymbol{F}^{\mathrm{d}} \\ \boldsymbol{M}^{\mathrm{d}} \end{bmatrix}. \tag{17}$$

Then, the virtual control input $\boldsymbol{\mu}_i$ is selected by projecting $\boldsymbol{\mu}_i^{\mathrm{d}}$ along $\boldsymbol{q}_i$, as follows:

$$\boldsymbol{\mu}_i = \boldsymbol{q}_i \boldsymbol{q}_i^\top \boldsymbol{\mu}_i^{\mathrm{d}}. \tag{18}$$

3.2. Design of perpendicular component

The objective of designing the perpendicular input is to apply the desired force to the payload by aligning $\boldsymbol{q}_i$ to the desired direction $\boldsymbol{q}_i^{\mathrm{d}} \in S^2$, which is defined as

$$\boldsymbol{q}_i^{\mathrm{d}} = \frac{\boldsymbol{\mu}_i^{\mathrm{d}}}{\|\boldsymbol{\mu}_i^{\mathrm{d}}\|}. \tag{19}$$

From this definition, the desired angular velocity of each cable $\boldsymbol{\omega}_i^{\mathrm{d}} \in \mathbb{R}^3$ is obtained from the kinematic equation as

$$\boldsymbol{\omega}_i^{\mathrm{d}} = \hat{\boldsymbol{q}}_i^{\mathrm{d}} \dot{\boldsymbol{q}}_i. \tag{20}$$

To achieve this alignment, we design the perpendicular component $\boldsymbol{u}_i^\perp$ of the control input. Before proceeding, we reformulate the equation of motion for the i-th link. Substituting Eq. (10) into Eq. (3), we obtain

$$\dot{\boldsymbol{\omega}}_i = -\frac{1}{l_i}\hat{\boldsymbol{q}}_i \boldsymbol{a}_i + \frac{1}{m_i l_i}\hat{\boldsymbol{q}}_i \left(\boldsymbol{u}_i^\perp + \boldsymbol{\Delta}_{x_i}^\perp\right). \tag{21}$$

To ensure the acceleration's effect on the dynamics at the cable's attachment point on the payload, the perpendicular component is designed as follows:

$$\boldsymbol{u}_i^\perp = -m_i \hat{\boldsymbol{q}}_i^2 \boldsymbol{a}_i + \tilde{\boldsymbol{u}}_i^\perp. \tag{22}$$

Here, the term $\tilde{\boldsymbol{u}}_i^\perp \in \mathbb{R}^3$ is an arbitrary input. This control law is formulated using a geometric PD-type approach, which is a standard PD-type controller for motion on a sphere given by

$$\begin{aligned} \tilde{\boldsymbol{u}}_i^\perp = &- m_i l_i \hat{\boldsymbol{q}}_i \left(-k_q \boldsymbol{e}_{q_i} - k_\omega \boldsymbol{e}_{\omega_i} - \left(\boldsymbol{q}_i \cdot \boldsymbol{\omega}_i^{\mathrm{d}}\right)\dot{\boldsymbol{q}}_i \right. \\ &\left. - \hat{\boldsymbol{q}}_i^2 \dot{\boldsymbol{\omega}}_i^{\mathrm{d}}\right) - \bar{\boldsymbol{\Delta}}_{x_i}^\perp. \end{aligned} \tag{23}$$

Here, $k_q, k_\omega > 0$ are positive gains, and $\boldsymbol{e}_{q_i}, \boldsymbol{e}_{\omega_i} \in \mathbb{R}^3$ are respectively the direction and angular velocity tracking error vectors defined as follows:

$$\boldsymbol{e}_{q_i} = \hat{\boldsymbol{q}}_i^{\mathrm{d}} \boldsymbol{q}_i, \quad \boldsymbol{e}_{\omega_i} = \boldsymbol{\omega}_i + \hat{\boldsymbol{q}}_i^2 \boldsymbol{\omega}_i^{\mathrm{d}}.$$

Then, Eq. (21) can be rewritten as

$$\dot{\boldsymbol{\omega}}_i = \frac{1}{m_i l_i}\hat{\boldsymbol{q}}_i \left(\tilde{\boldsymbol{u}}_i^\perp + \boldsymbol{\Delta}_{x_i}^\perp\right). \tag{24}$$

3.3. Disturbance estimation

We estimate the disturbances using integral actions following the approach in [8]. This method is carried out by compensating for the cumulative impact of errors, which is aimed for the tracking errors to converge to zero based on Lyapunov stability approaches [8]. However, it should be noted that asymptotic convergence of the estimation error is not guaranteed. The update law for the disturbance estimate is given by

$$\dot{\bar{\boldsymbol{\Delta}}}_{x_L} = \frac{\gamma_{x_L}}{m_L}\left(\dot{\boldsymbol{e}}_{x_L} + c_x \boldsymbol{e}_{x_L}\right), \tag{25}$$

$$\dot{\bar{\boldsymbol{\Delta}}}_{R_L} = \gamma_{R_L}\left(\boldsymbol{e}_{\Omega_L} + c_R \boldsymbol{e}_{R_L}\right), \tag{26}$$

$$\begin{aligned} \dot{\bar{\boldsymbol{\Delta}}}_{x_i} = &\gamma_{x_i} \boldsymbol{q}_i \boldsymbol{q}_i^\top \left(\frac{1}{m_L}\left(\dot{\boldsymbol{e}}_{x_L} + c_x \boldsymbol{e}_{x_L}\right) \right. \\ &\left. - \boldsymbol{R}_L \hat{\boldsymbol{\rho}}_i \left(\boldsymbol{e}_{\Omega_L} + c_R \boldsymbol{e}_{R_L}\right)\right) - \frac{\gamma_{x_i}}{m_i l_i}\hat{\boldsymbol{q}}_i \left(\boldsymbol{e}_{\omega_i} + c_q \boldsymbol{e}_{q_i}\right). \end{aligned} \tag{27}$$

Here, $c_x, c_R, c_{q_i} \in \mathbb{R}$ are positive constants and $\gamma_{x_L}, \gamma_{R_L}, \gamma_{x_i} \in \mathbb{R}$ are integral gains.

4. COLLISION AVOIDANCE METHOD

We present our control approach to address the problem of potential collision between the multiple UAVs. The method constrains the cable angles using a conic CBF [14].

4.1. Collision between UAVs

To detect collision between the UAVs or between a UAV and a neighboring cable, we define the minimum distance D, as illustrated in Fig. 3. The distance D is defined as

$$D = \begin{cases} \|\boldsymbol{x}_{i(x,y)} - \boldsymbol{x}_{j(x,y)}\| - s & \text{if } |x_{i(z)} - x_{j(z)}| < w \\ \|\boldsymbol{p}_{i(x,y)} - \boldsymbol{x}_{j(x,y)}\| - \frac{s}{2} & \text{if } |x_{i(z)} - x_{j(z)}| > w \end{cases}$$

Here s and w are the size and the thickness of the UAV. For any vector $\boldsymbol{A} = [x\ y\ z]^\top$, we define $\boldsymbol{A}_{(x,y)}$ as the its projection onto the xy-plane, and $\boldsymbol{A}_{(z)}$ as the z-axis component. Additionally, $\boldsymbol{p}_i \in \mathbb{R}^3$ represents the position of the cable at the same height as the neighboring UAV.

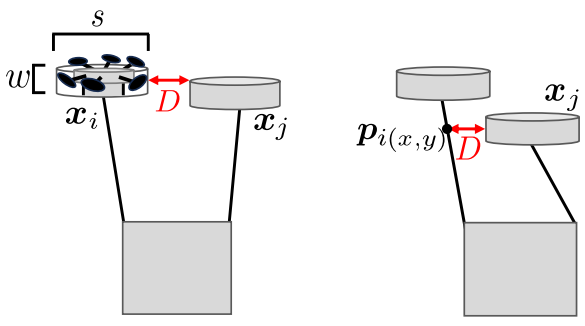

(a) $|\boldsymbol{x}_{i(z)} - \boldsymbol{x}_{j(z)}| < w$ (b) $|\boldsymbol{x}_{i(z)} - \boldsymbol{x}_{j(z)}| > w$

Fig. 3: Image of the distance between adjacent UAVs.

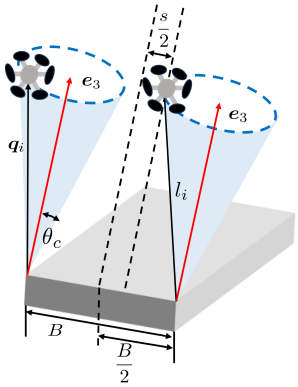

Fig. 4: Conic constraints.

4.2. Constaints based on a conic CBF

As shown in Fig. 4, we consider a cone with a restricting angle $\theta_c > 0$ with the unit vector $\boldsymbol{e}_3$ as the conic axis.

First, we determine θ_c. As a sufficient condition for ensuring $D > 0$, the angle θ_c is determined such that each cable satisfies as follows:

$$l_i \tan(\theta_c) < \frac{1}{2}(B - s). \tag{28}$$

Here, B is the smaller of the width and depth of the payload. Furthermore, the value of B is chosen in this way to impose the collision avoidance condition with respect to the more restrictive side of the payload. As B becomes smaller, it becomes more difficult to maintain sufficient spacing between UAVs, and thus the allowable minimum distance D also decreases. Based on θ_c, the constraint keeps the angle of each cable within θ_c is expressed as

$$\boldsymbol{q}_i^\top \boldsymbol{e}_3 \geq \cos\theta_c. \tag{29}$$

To achieve this requirement during trajectory tracking, we introduce a constrained optimization based control. Following Eq. (29), we define a conic CBF $h_i \in \mathbb{R}$ as

$$h_i(\boldsymbol{q}) = \boldsymbol{q}_i^\top \boldsymbol{e}_3 - \cos\theta_c. \tag{30}$$

In this case, the safe set is represented as follows, and by satisfying the CBF condition in Eq (30), a safe set C becomes forward invariant.

$$C = \{\boldsymbol{q}_i \in S^2 | h_i(\boldsymbol{q}) \geq 0\}. \tag{31}$$

The approach of this work is a modification of the method proposed in [12], adapted to represent the attitude of the cable. This condition ensures that each cable maintains an angle less than θ_c from the vertical direction. However, this constraint cannot be directly applied because the relative degree of the CBF h_i is 2. Therefore, to derive the input conditions for the cable angle constraints, we take the second-order time derivative of the conic CBF and introduce a High-Order CBF [15].

In this paper, we adopt simple proportional functions with gains $\alpha, \beta > 0$ as an extended extended class $\mathcal{K}$ function. Based on Eq. (29), the CBF condition for angular acceleration is obtained.

$$\begin{aligned}
&\ddot{h}_i + (\alpha+\beta)\dot{h}_i + \alpha\beta h_i \\
&= \ddot{\boldsymbol{q}}_i^\top \boldsymbol{e}_3 + \alpha\dot{\boldsymbol{q}}_i^\top \boldsymbol{e}_3 + \beta\left(\boldsymbol{q}_i^\top \boldsymbol{e}_3 + \alpha\left(\boldsymbol{q}_i^\top \boldsymbol{e}_3 - \cos\theta_c\right)\right) \\
&= (\dot{\hat{\boldsymbol{\omega}}}_i \boldsymbol{q}_i)^\top \boldsymbol{e}_3 + (\hat{\boldsymbol{\omega}}_i^2 \boldsymbol{q}_i)^\top \boldsymbol{e}_3 + (\alpha+\beta)(\hat{\boldsymbol{\omega}}_i \boldsymbol{q}_i)^\top \boldsymbol{e}_3 \\
&\quad + \alpha\beta(\boldsymbol{q}_i^\top \boldsymbol{e}_3 - \cos\theta_c) \geq 0.
\end{aligned} \tag{32}$$

Using Eq. (24), this constraint can be rewritten with the control input $\tilde{\boldsymbol{u}}_i^\perp$ as

$$\begin{aligned}
&\frac{\boldsymbol{e}_3^\top \hat{\boldsymbol{q}}_i^2}{m_i l_i}\left(\tilde{\boldsymbol{u}}_i^\perp - \hat{\boldsymbol{q}}_i^2 \boldsymbol{\Delta}_{x_i}\right) = \frac{\boldsymbol{e}_3^\top}{m_i l_i}\left(\hat{\boldsymbol{q}}_i^2 \tilde{\boldsymbol{u}}_i^\perp + \hat{\boldsymbol{q}}_i^2 \boldsymbol{\Delta}_{x_i}\right) \\
&\leq (\hat{\boldsymbol{\omega}}_i^2 \boldsymbol{q}_i)^\top \boldsymbol{e}_3 + (\alpha+\beta)(\hat{\boldsymbol{\omega}}_i \boldsymbol{q}_i)^\top \boldsymbol{e}_3 \\
&\quad + \alpha\beta(\boldsymbol{q}_i^\top \boldsymbol{e}_3 - \cos\theta_c).
\end{aligned} \tag{33}$$

Since the disturbance is unknown, the expression is reformulated using the bound of the size of the disturbance, denoted by δ, which satisfies $\max \|\boldsymbol{\Delta}_{x_i}\| \leq \delta$ and we assume that the bound δ is known by a prior experimental test or supplementary information. Then, the following inequality is used

$$\begin{aligned}
\boldsymbol{e}_3^\top \hat{\boldsymbol{q}}_i^2 \boldsymbol{\Delta}_{x_i} &= \boldsymbol{e}_3^\top \left(\boldsymbol{I}_3 - \boldsymbol{q}_i^\top \boldsymbol{q}_i\right) \boldsymbol{\Delta}_{x_i} \\
&= \boldsymbol{e}_3^\top \boldsymbol{\Delta}_{x_i} + \left(\boldsymbol{e}_3^\top \boldsymbol{q}_i\right)\left(\boldsymbol{q}_i^\top \boldsymbol{\Delta}_{x_i}\right) \\
&\leq \|\boldsymbol{e}_3\|\|\boldsymbol{\Delta}_{x_i}\| + \left(\|\boldsymbol{e}_3^\top\|\|\boldsymbol{q}_i\|\right)\left(\|\boldsymbol{q}_i\|\|\boldsymbol{\Delta}_{x_i}\|\right) \\
&= 2\|\boldsymbol{\Delta}_{x_i}\| \leq 2\delta.
\end{aligned} \tag{34}$$

Therefore, the constraint can be rewritten as follows:

$$\begin{aligned}
\frac{\boldsymbol{e}_3^\top \hat{\boldsymbol{q}}_i^2}{m_i l_i}\tilde{\boldsymbol{u}}_i^\perp &\leq (\hat{\boldsymbol{\omega}}_i^2 \boldsymbol{q}_i)^\top \boldsymbol{e}_3 + (\alpha+\beta)(\hat{\boldsymbol{\omega}}_i \boldsymbol{q}_i)^\top \boldsymbol{e}_3 \\
&\quad + \alpha\beta(\boldsymbol{q}_i^\top \boldsymbol{e}_3 - \cos\theta_c) - \frac{2\delta}{m_i l_i}.
\end{aligned} \tag{35}$$

4.3. Collision avoidance controller

Based on the constraint (35), we propose a method for avoiding collision between the UAVs as a solution of the quadratic programming: quadratic programming.

$$\begin{aligned}
(\tilde{\boldsymbol{u}}_i^\perp)^* = \underset{\tilde{\boldsymbol{u}}_i^\perp \in \mathbb{R}^3}{\operatorname{argmin}} &\|\tilde{\boldsymbol{u}}_i^\perp - \tilde{\boldsymbol{u}}_{i,\mathrm{nom}}^\perp\|^2 \\
\text{s.t.} \quad &\text{Constraint (35)}
\end{aligned} \tag{36}$$

where $\tilde{\boldsymbol{u}}_{i,\mathrm{nom}}^\perp$ is nominal perpendicular input, given by Eq. (22). Following this solution, the optimal perpendicular control input $(\tilde{\boldsymbol{u}}_i^\perp)^*$ is obtained by minimizing the squared Euclidean distance to the nominal input $\tilde{\boldsymbol{u}}_{i,\mathrm{nom}}^\perp$. This allows the UAV to apply the desired force to the payload while ensuring that the cable angle remains within the specified limit.

In summary, the total control input for each UAV is given as follows:

$$\boldsymbol{u}_i = \boldsymbol{u}_i^\parallel + (\boldsymbol{u}_i^\perp)^* = \boldsymbol{u}_i^\parallel - m_i \hat{\boldsymbol{q}}_i^2 \boldsymbol{a}_i + (\tilde{\boldsymbol{u}}_i^\perp)^*. \tag{37}$$

5. SIMULATION

5.1. Parameter setting

In this simulation, we define the restricting angle $\theta_c = \pi/16$ [rad]. The gravitational acceleration is set to $g = 9.81$ [m/s^2]. The mass of the payload is $m_L = 1.8$ [kg], and the rectangular payload's width, depth, and height are 0.8 [m], 0.6 [m], and 0.4 [m]. Inertia matrix of the payload is $J_L = \mathrm{diag}[0.0780\ 0.1200\ 0.1500]$ [kg $\cdot$ m^2]. The mass, size, and thickness of three UAVs are common given $m_i = 1.0$ [kg], $s_i = 0.2$ [m], $w = 0.15$ [m]. The length of all the cables is set as $l_i = 1.0$ [m], and they are attached to the following points of the payload:

$$\boldsymbol{\rho}_1 = [0.4\ 0\ 0.2]^\top \text{ [m]},\ \boldsymbol{\rho}_2 = [-0.4\ 0.3\ 0.2]^\top \text{ [m]},$$
$$\boldsymbol{\rho}_3 = [-0.4\ -0.3\ 0.2]^\top \text{ [m]}.$$

The desired trajectory of the payload is given as

$$\boldsymbol{x}_L^{\mathrm{d}}(t) = [1.0t\ 2.5\sin(0.2\pi t)\ 0]^\top \text{ [m]}.$$

Then, the desired attitude of the payload is chosen so that the orientation around the vertical axis (yaw angle) faces the direction of motion while the other attitudes are parallel to the ground (roll and pitch angles are 0). Initial conditions are chosen as $\boldsymbol{x}_L(0) = \boldsymbol{0}_{3\times1}$ [m], $\boldsymbol{v}_L(0) = \boldsymbol{0}_{3\times1}$ [m/s], $\boldsymbol{R}_L(0) = \boldsymbol{I}_3$, $\boldsymbol{\Omega}_L(0) = \boldsymbol{0}_{3\times1}$ [rad/s], $\boldsymbol{x}_i(0) = \boldsymbol{0}_{3\times1}$ [m], $\boldsymbol{v}_i(0) = \boldsymbol{0}_{3\times1}$ [m/s], $\boldsymbol{q}_i(0) = \boldsymbol{e}_3$, $\boldsymbol{\omega}_i(0) = \boldsymbol{0}_{3\times1}$ [rad/s] $^\forall i$. Moreover, the disturbances are set as

$$\begin{aligned}\boldsymbol{\Delta}_{x_L} &= [0.3{+}0.25\sin(1.8t)\ 0.2 + 0.2\cos(2.2t)\\ &\qquad 0.2 - 0.2\sin(1.9t)]^\top,\\ \boldsymbol{\Delta}_{x_i} &= [0.25{+}0.15\sin(2.1t)\ 0.2 - 0.1\cos(1.8t)\\ &\qquad 0.1 + 0.1\sin(2.3t)]^\top,\\ \boldsymbol{\Delta}_{\boldsymbol{R}_L} &= [0.3{+}0.2\cos(1.9t)\ 0.15 + 0.15\sin(1.2t)\\ &\qquad -0.1 - 0.05\sin(1.6t)]^\top.\end{aligned}$$

Therefore, since $\max\|\boldsymbol{\Delta}_{x_i}\| \approx 0.48$, we set $\delta = 0.5$.

5.2. Result

The simulation results are shown in Figs. 5-10. Figs. 5-8 show the time responses of the position and attitude of the payload. Fig. 9 shows the time responses of the distance D between $\boldsymbol{\rho}_2$ and $\boldsymbol{\rho}_3$ with the shortest distances of the cable's attachment point on the payload. Moreover, Fig. 10 shows the time response of h_i, which indicates how much the cable is tilted with respect to the axis $\boldsymbol{e}_3$.

From Figs. 5-8, it can be observed that the position and orientation of the payload are well maintained under disturbances, regardless of the application of the CBF. As shown in Fig. 9(a), the UAVs collide when the CBF is not applied. However, when the CBF is applied, as shown in Fig. 9(b), the distance D is always maintained above 0, which means no collision occurs. This is because as shown in Fig. 10(a), the cables move without restriction before the CBF was applied, whereas, as depicted in Fig. 10(b), the angle of each cable is restricted.

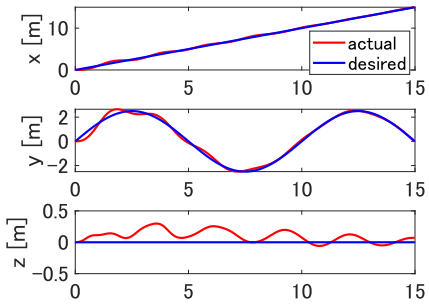

Fig. 5: Position of payload without CBF.

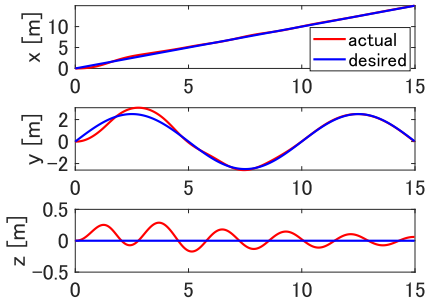

Fig. 6: Position of payload with CBF.

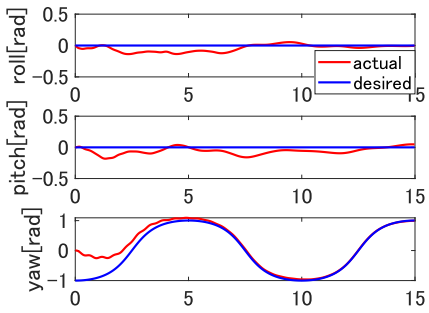

Fig. 7: Attitude of payload without CBF.

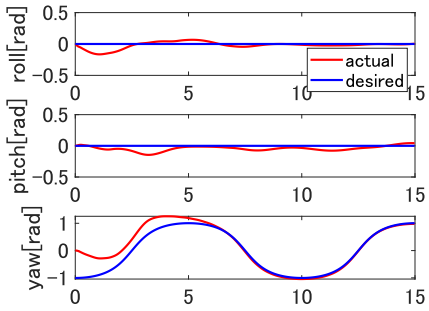

Fig. 8: Attitude of payload with CBF.

6. CONCLUTION

In this paper, we proposed a method to avoid collision between the multiple UAVs in a load transportation sys-

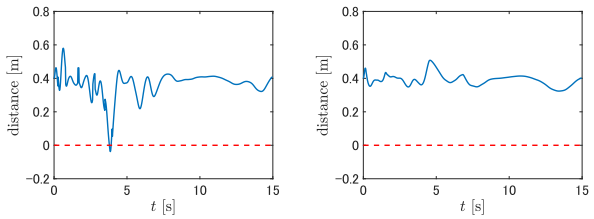

(a) without CBF. (b) with CBF.

Fig. 9: Distance D between UAV2 and UAV3.

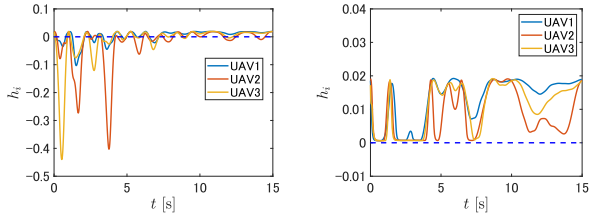

(a) without CBF. (b) with CBF.

Fig. 10: Time response of h_i.

tem using three UAVs and demonstrated its effectiveness through simulations. The key feature of this research is the use of a conic CBF to construct constraints, allowing the system to transport a load while ensuring the safety of multiple UAVs. For future work, we plan to utilize the relative cable vector because it is often the case that the more one cable tilts, the greater the allowable angle for the others becomes. Additionally, we intend to test the proposed system through actual experiments.

REFERENCES

[1] J. Besada, L. Bergesio, I. Campaña, D. Vaquero-Melchor, J. López-Araquistain, A. Bernardos, and J. Casar, "Drone mission definition and implementation for automated infrastructure inspection using airborne sensors", *Sensors*, Vol. 18, No. 4 p. 1170, 2018.

[2] Q. Lindsey, D. Mellinger, and V. Kumar, "Construction with quadrotor teams", *Autonomous Robots*, Vol. 33, pp. 323–336, 2012.

[3] I. Mademlis I. Mademlis, V. Mygdalis, N. Nikolaidis, M. Montagnuolo, F. Negro, A. Messina, and I. Pitas, "High-level multiple-UAV cinematography tools for covering outdoor events", *IEEE Transactions on Broadcasting*, Vol. 65, No. 3, pp. 627–635, 2019.

[4] D. Mellinger, Q. Lindsey, M. Shomin, and V. Kumar, "Design, modeling, estimation and control for aerial grasping and manipulation", *in Proceedings of the 2011 IEEE/RSJ International Conference on Intelligent Robots and Systems*, pp. 2668–2673, 2011.

[5] Paul E. I. Pounds, "Grasping from the air: Hovering capture and load stability", *in proceeding of the 2011 IEEE International Conference on Robotics and Automation*, pp. 2491–2498, 2011.

[6] S. Yang and B. Xian, "Energy-based nonlinear adaptive control design for the quadrotor UAV system with a suspended payload", *IEEE Transactions on Industrial Electronics*, Vol. 67, No. 3, pp. 2054–2064, 2020.

[7] T. Lee, K. Sreenath, and V. Kumar, "Geometric control of cooperating multiple quadrotor UAVs with a suspended payload", *in Proceedings of the 52nd IEEE Conference on Decision and Control*, pp. 5510–5515, 2013.

[8] T. Lee, "Geometric control of quadrotor UAVs transporting a cable-suspended rigid body", *IEEE Transactions on Control Systems Technology*, Vol. 26, No. 1, pp. 255–264, 2018.

[9] Y. Wang, G. Yu, W. Xie, W. Zhang and C. Silvestre, "Robust cooperative transportation of a cable-suspended payload by multiple quadrotors featuring cable-reconfiguration capabilities", *IEEE Transactions on Intelligent Transportation Systems*, Vol. 25, No. 9, pp. 11833–11843, 2024.

[10] J. Geng and J. W. Langelaan, "Cooperative transport of a slung load using load-leading control", *IEEE Transactions on Intelligent Transportation Systems*, Vol. 43, No. 7, pp. 1313–1331, 2020.

[11] J. Cai and B. Xian, "Robust hierarchical geometry control for the multiple UAVs aerial transportation system with a suspended payload", *Nonlinear Dynamics*, Vol. 43, No. 7, pp. 4551–4571, 2024.

[12] Y. Tadokoro, T. Ibuki and M. Sampei, "Joint optimization of geometric control and structure of a fully-actuated hexrotor based on an analytic HJBE solution", *in Proceedings of the 57th IEEE Conference on Decision and Control*, pp. 1186–1191, 2018.

[13] T. Lee, "Computational geometric mechanics and control of rigid bodies", Ph.D. *Dissertation*, University of Michigan, 2008.

[14] T. Ibuki, S. Wilson, A. D. Ames, and M. Egerstedt, "Distributed collision-free motion coordination on a sphere: a conic control barrier function approach", *IEEE Control System Letters*, Vol. 4, No. 4, pp. 976–981, 2020.

[15] W. Xiao and C. Belta, "Control barrier function for systems with high relative degree", *in Proceedings of the 58th IEEE Conference on Decision and Control*, pp. 474-479, 2019.